John von Neumann Institute for Computing

Hydrodynamics of Active Mesoscopic Systems

J. Elgeti, G. Gompper

published in

NIC Symposium 2008,
G. Münster, D. Wolf, M. Kremer (Editors),
John von Neumann Institute for Computing, Jülich,
NIC Series, Vol. **39**, ISBN 978-3-9810843-5-1, pp. 53-62, 2008.

http://www.fz-juelich.de/nic-series/volume39

Hydrodynamics of Active Mesoscopic Systems

Jens Elgeti and Gerhard Gompper

Institut für Festkörperforschung
Research Centre Jülich, 52425 Jülich, Germany
E-mail: {j.elgeti, g.gompper}@fz-juelich.de

The dynamics of active mesoscopic systems is studied by multi-particle collision dynamics, a mesoscale hydrodynamic simulation technique. Sperm motion serves as a model system par excellence. The sperm tail is modelled by a crane-like structure. It is shown that helical trajectories are generated by a chiral structure of the sperm. The connection between sperm geometry and parameters of the trajectory is determined.

1 Introduction

Many eucaryotic cells and bacteria move and navigate actively in their environment. Some well-known examples are E.coli, which swims by a rotating helical filament in search for food, fibroblasts, which crawl to close a wound, and sperm cells, which swim with a beating flagellum to find the egg. The catalog of cell motion is long, each form especially suited for the given task of the cell.

Cell crawling, where cells adhere to surfaces and extend filopodia to pull themselves forward, is a slow process, with typical velocities around 10 $\mu m/min$. We are interested here in the faster forms of mesoscopic swimming. Sperm cells are the model systems par excellence, with swimming velocities around 50 $\mu m/s$. Swimming on mesoscopic length scales of nano- to micro-meters, is a lot different than on the macroscopic length scales familiar to us[1]. Hydrodynamics is in general described by the Navier Stokes equation. The Reynolds number $Re = \rho u l/\eta$, where ρ is the density and η the viscosity of the fluid, and u and l are characteristic length and velocity scales, determines the importance of the non-linear inertia terms. In the low Reynolds number regime, viscous forces dominate over inertia, leading to the linear and time-reversible Stokes equation. The consequences of a low Reynolds number are quite surprising. For example, a coloured drop can be deposited in a high-viscosity fluid between two concentric cylinders. When the inner cylinder is turned several times to mix the fluids, and susequently the same number of times in the opposite direction, the result is *not* a homogeneous mixture – instead the drop is reformed![2]. This effect renders time-reversible swimming mechanisms impossible. A nice review of *swimming at low Reynolds numbers* can be found in Ref.[1].

Sperm cells propel themselves forward by a snake-like motion of their tail, the flagellum, towards the egg. The best-known example is clearly human sperm, but almost all higher species, from the sea urchin to the elephant, produce sperm. These sperm all look remarkably alike. The flagellum may have a different length, but its underlying cytoscelatal structure is well preserved throughout animal live. The direction of sperm motion is controlled by chemotaxis, and has been studied extensively. Recently, the biochemical signaling cascade of chemotaxis of Sea Urchin spermatozoa has been unraveled[3]. Our work is focused on the *hydrodynamic* effects in these systems.

Cilia are hair-like extensions from the cell that propel fluid by a whip-like motion. Cilia are even more abundant in nature than sperm. The Paramecium is covered with thousands of cilia to propel it through the fluid, the mammalian lung is equipped with cilia to propel mucus out of the system, and in the female reproductive tract cilia move the egg.

Typically cilia appear in large arrays, so that hydrodynamic interactions between multiple active compounds play an essential role. It has been proposed, but not yet proven, that hydrodynamic interactions lead to metachronal waves, a self organized pattern found on ciliated surfaces. In a large array, cilia do not beat synchronously or randomly, but in a well defined wave-like pattern.

Activity on mesoscopic length scales is what is uniting these systems. They consist of intrinsically active, micrometer-sized filaments in fluid suspension. Activity is not imposed by outside fields, but generated within the objects themselves.

2 Mesoscale Hydrodynamics

Hydrodynamics plays an essential role in mesoscopic systems. Clearly the systems are too large (several μm) to model the water explicitly. Furthermore the hydrodynamics has only to be resolved on the relevant length scales of the system. This calls for a coarse-grained description of the fluid.

Several mesoscale simulation techniques to describe the hydrodynamics of complex fluids have been proposed in recent years, such as Lattice-Boltzmann, Dissipative Particle Dynamics and Multi-Particle-Collision Dynamics. The basic idea in all these approaches is to employ a highly simplified dynamics on the microscale, but to respect the relevant conservation laws for mass, momentum and energy, such that hydrodynamical behaviour emerges naturally on larger length scales.

Multi-Particle Collision Dynamics (MPC) is one such technique[4–6]. In MPC, the fluid is represented by N point particles in continuous space. The particles travel with continuous velocities, and interact with a coarse-grained multi-particle interaction. The dynamics evolves in two steps. In the *streaming step*, the particles move ballistically for a collision-time h,

$$\vec{r}_i(t+h) = \vec{r}_i(t) + h\vec{v}_i(t). \tag{1}$$

In the *collision step*, the particles are sorted into the cells of a cubic lattice with lattice constant a and their velocities, relative to the centre-of-mass velocity of all particles in the cell, are rotated around a random axis by an angle α,

$$\vec{v}_i(t+h) = \vec{v}_{cm}(t) + \mathfrak{R}(\vec{v}_i(t) - \vec{v}_{cm}(t)), \tag{2}$$

where $\mathfrak{R}$ is a rotation matrix. The direction of rotation is chosen independently for each box at each time step, while the rotation angle is typically constant and used as a parameter to tune viscosity and Schmidt number $S_c = \eta/\rho D$, the ratio of momentum to mass diffusivity (D is the diffusion constant). It has been shown that large collision angles and small time steps are best suited for simulating fluid-like behaviour at low Reynolds numbers[7,8].

To ensure Galilean invariance, the collision grid has to be shifted between subsequent collision steps[6,9].

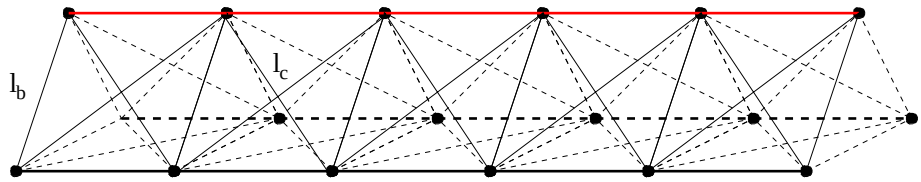

Figure 1. The axoneme is modelled as three polymer rods, interconnected by harmonic springs. Bond length $l_b = a/2$, $l_c = 1/\sqrt{2}$.

Both, the collision step and the streaming step conserve momentum and energy explicitly, so that hydrodynamic behaviour emerges automatically on large length scales. Due to the particle-based description of the fluid, coupling to other embedded mesoscale objects is straightforward. In particular Molecular Dynamics is well suited to simulate immersed objects like polymers or vesicles.

One big advantage of this method is its computational efficiency, due to the simple interactions between the particles. Furthermore, the largest part of the iterations are independent of each other and the interactions are local, thus causing the algorithm to scale very well on parallel machines.

This method is by now widely in use, for example in studies of polymers and star-polymers under shear flow[10] and vesicles or red blood cells in flow[11,12].

3 Sperm Model

Sperm cells consist of three parts. The head, containing the nucleus where the genetic information is stored, the beating tail that propels the sperm through the fluid and the midpiece in between. Of course more structures and substructures can be identified, but these are not important for their hydrodynamic properties.

The beating tail, i.e. the axoneme, can be well described as an active elastic rod. We model the axoneme with a crane-like structure (see Fig 1). Three semi-flexible rods are interconnected by springs to obtain a three-dimensional structure with well-suited elastic properties. The three-fold structure allows to impose an internal-active and directed bending by changing the rest lengths of the individual bonds, thus imposing a spontaneous directed curvature onto the structure.

The final tail structure contains 100 monomeres per rod, which are thus $S_l = 50\,a$ long. A spherical head is attached in front. For propulsion, a propagating sine-wave is imposed on the tail behind a short ($10a$) passive midpiece. In experiments, helical motion of sperm in a bulk fluid is observed, requesting some form of chirality of the sperm due to symmetry reasons. To impose this chirality, the midpiece can be bent by a predefined bending parameter b, see Fig. 4. The bending paramter b measures how much one rod of the midpiece is shortened, relative to its straight length. At $b = 9\%$ the midpiece forms approximately a quarter circle. Since this bent is imposed on a different rod than the beat pattern, it bends the head out of the beating plane, creating chirality.

Coupling to hydrodynamics is done by immersing the structure in a MPC fluid and including monomers in the collision step, as suggested in Ref.[13] for polymers. To sufficiently resolve the hydrodynamics in MPC, the beat amplitude of the tail has to exceed a

few MPC collision boxes. This requires a large sperm structure of length $S_l = 50\,a$, and correspondingly large simulation boxes. For bulk simulations, we simulate 70^3 collision boxes with periodic boundary conditions. Because each box contains 10 fluid particles, this corresponds to 3.5 million particles, and consequently demands large computational resources.

4 Hydrodynamics of Thin Rods

The tail of a sea urchin spem cell is $50\mu m$ long, and less than $0.5\mu m$ in diameter. The hydrodynamics of the tail should therefore be well described by a sequence of thin rods. Thin rods have an anisotropic friction with the solvent, where the friction force perpendicular to the rod, $\vec{F}_\perp$ is larger then parallel, $\vec{F}_\parallel$.

Intuitively it is obvious that dragging a rod perpendicular to its orientation is more difficult than parallel, and the physical origin of this behaviour is easy to understand. If moved parallel to its orientation, most of the rod can travel in the wake of the tip, thus reducing friction.

We define rod-drag coefficients for Stokes flow by

$$F_\parallel = \gamma_\parallel v_\parallel \tag{3}$$

$$F_\perp = \gamma_\perp v_\perp \tag{4}$$

with the subscript $\parallel$ for vector components parallel to the rod, and $\perp$ for perpendicular components. These friction coefficients are related to the diffusion coefficients $D_{\parallel,\perp}$ via

$$\gamma_{\parallel,\perp} = \frac{k_B T}{D_{\parallel,\perp}} \tag{5}$$

Calculating the diffusion coefficients for a rod-like colloid of finite length is not trivial, but approximations can be found in the literature. Tirado, Martinez and Garcia de la Torre[14] reviewed some theoretical approaches. The different theories agree on

$$\frac{2\pi\eta L_r D_\parallel}{k_B T} = \ln(L_r/d_r) + \nu_\parallel \tag{6}$$

$$\frac{4\pi\eta L_r D_\perp}{k_B T} = \ln(L_r/d_r) + \nu_\perp. \tag{7}$$

where L_r is the length, and d_r the diameter of the rod. Differences between theories are found concerning the correction functions $\nu_{\perp/\parallel}$. One approximation for $2 < L_r/d_r < 30$ is

$$\nu_\perp = 0.839 + 0.185 d_r/L_r + 0.233\,(d_r/L_r)^2 \tag{8}$$

$$\nu_\parallel = -0.207 + 0.980 d_r/L_r - 0.133\,(d_r/L_r)^2 \tag{9}$$

These results can be used to calculate the swimming velocity of sperm. Gray and Hancock[15] used this approach to calculate the swimming velocity of sperm cells. After assuming a sine-shaped beat-pattern, $\gamma_\perp = 2\gamma_\parallel$, and some other approximations, they obtained the swimming speed

$$\bar{v}_x = \frac{\omega\pi b^2}{\lambda}\left(1 + \frac{4\pi^2 b^2}{\lambda^2} - \sqrt{1 + \frac{2\pi^2 b^2}{\lambda^2}}\frac{C_H}{n\lambda\gamma_\parallel}\right)^{-1} \tag{10}$$

where ω is the angular frequency, λ the wavelength and b the amplitude of the beat. The number of waves present on the tail is denoted by n, C_H is the drag coefficient of the head. For a spherical head of radius R_h and a thin tail of radius d, it is possible to approximate

$$\frac{C_H}{\gamma_\parallel} = 3R_h \left[\left(\log \frac{d}{2\lambda} \right) + \frac{1}{2} \right]. \tag{11}$$

Because a pre-defined beat shape has been used, the viscosity η does not influence the swimming speed.

Like the swimming velocity of sperm, other mesoscopic systems of slender bodies can be described in this fashion. Always, either the assumption $\gamma_\perp = 2\gamma_\parallel$ or the ratio $\gamma_\perp/\gamma_\parallel$ play an essential role. Sperm, for example, would not move if $\gamma_\perp = \gamma_\parallel$. This shows the importance and effects of the anisotropic friction of thin rods. To compare our results to slender body theory, and as a suitability test of our model, we performed simulations to calculate $\gamma_\perp$ and $\gamma_\parallel$ in an MPC fluid.

For this purpose we keep the structure, presented above as the sperms tail, in the centre of a simulation box and expose it to a constant flow. The friction coefficients are determined by averaging the forces on the structure. A uniform flow field imposed sufficiently far from the rod by assigning Gaussian-distributed velocities, with an average of $\bar{v}$ in the flow direction, to the solvent particles in a layer of thicknes $1a$ perpendicular to the flow direction.

The drag force is found to be linear with $\bar{v}$ at least up to $\bar{v} \approx 0.3\sqrt{m/k_bT}$. We chose $\bar{v} = 0.1\sqrt{m/k_bT}$, well within the linear regime for the remaining simulations.

Fig. 2 shows as an example the friction coefficients $\gamma_\parallel$ and $\gamma_\perp$ as a function of scaled inverse linear system size (L_r/S). To determine the friction coefficients at infinite dilution,

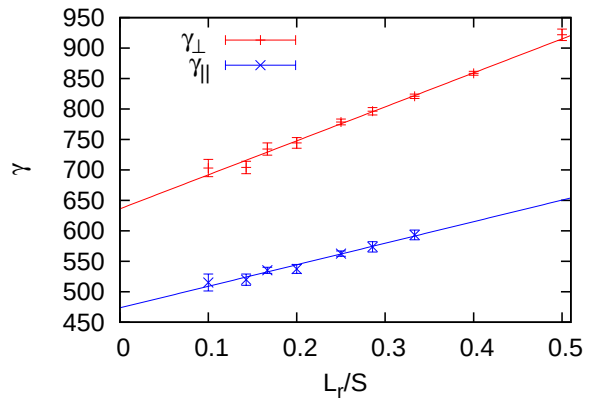

Figure 2. Friction coefficients $\gamma_\parallel$ and $\gamma_\perp$ as a function of scaled inverse linear system size L_r/S. System size S^3 varies between $(20\,a)^3$ and $(100\,a)^3$. Rod length is $10\,a$. MPC parameters are $\alpha = 130°, \rho = 10, h = 0.05\sqrt{ma^2/k_BT}$.

we fitted a linear function to the data (see Fig. 2), and used the extrapolation to infinite system size. The strong finite-size effects demand large systems and limit the range of

accessible rod lengths. The largest simulated systems used are for rods with a length of $20\,a$ with 110^3 boxes, or 13 million particles.

Considering the strong finite-size effects, and that the polymer rods are weakly penetrable for the fluid, the agreement with theory is surprisingly good (see Fig. 3). The fit in

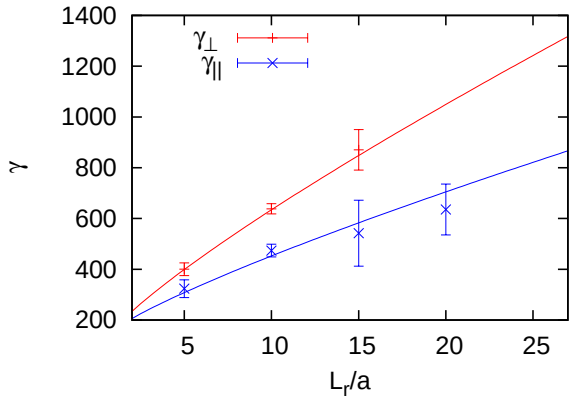

Figure 3. Friction coefficients $\gamma_{\|}$ and $\gamma_{\perp}$ as a function of rod length L_r. The solid line is a fit of the theory (Eqs.(6) and (7)) to the data of $\gamma_{\perp}$, resulting in $d_r \approx 0.9\,a$. This value was then also used to plot $\gamma_{\|}$. Points are results of finite-size fits, as described in the text.

Fig. 3 resulted in a rod diameter of $d_r \approx 0.9\,a$, which is quite reasonable. Furthermore, we see from Fig. 3 that at these low aspect ratios $\gamma_{\perp}/\gamma_{\|} < 2$. Note that also for sea urchin sperm tails, $L_r/d_r \approx 100$. The effective aspect ratio is considerably smaller due to the wave length $\lambda < L_r$.

5 Sperm Dynamics

We present here our results for bulk motion of sperm cells. Our aim is to investigate the effect of midpiece curvature and sperm chirality on the bulk motion. In bulk fluid we observe helical as well as almost straight trajectories, depending on the degree of chirality. Weakly bent sperm swim on a narrow helix. The tail is always close to the trajectory, just the head performs some sideways motions. Strongly bent sperm swim in a larger helix with the head near the centre of the helix and the tail pointing outward (see Fig. 4).

Besides its position and orientation in space, a helix has two independent parameters; typically these are the pitch p and the radius r. Additionally the sperm cells move with a velocity v on these helical trajectories. Some of these parameters are more prone to thermal fluctuations then others. We found that the curvature c, the tangential velocity v and the rotation frequency ω are the most reliable observables (see Fig. 5). Other parameters, for example the helix radius r, the velocity along the centreline v_z and the pitch p are connected to the tangential velocity v, angular frequency ω and curvature c via

$$r = \frac{cv^2}{\omega^2} \qquad v_z = \pm\sqrt{v^2 - c^2v^4} \qquad p = v_z 2\pi/\omega, \tag{12}$$

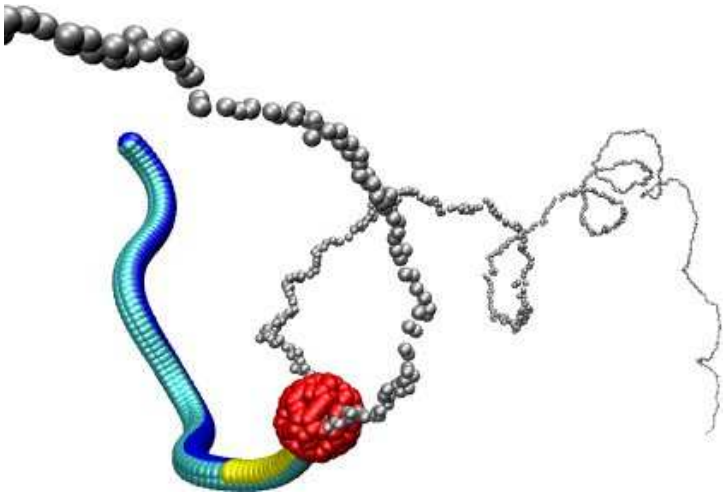

Figure 4. Visualization of a sperm motion in bulk fluid. In the beating tail the length of the blue rod is changed to impose a sinusoidal bending wave. At the tip a spherical head (red) is attached. In between we add a midpiece, that, in this case, is bend by shortening the yellow rod by 6%. At large enough bending parameters the elastic sperm twists on the axoneme, creating a strong bend. In this case, the twist is locatet approximatly at the kink in the bottom left corner of the picture. Without walls this sperm swims in a helical motion, visualized as the trajectory of the sperms head in gray spheres. Visualization using VMD[16]

and thus can be calculated from the data presented in Fig. 5.

The tangential velocity v is fairly independent of the bending parameter, with a velocity around $v \approx 0.02\, S_l/\tau_b$, decreasing by about 20% for strongly asymmetric sperm. Here τ_b is the beating period of the sperm.

The curvature follows a sigmoidal function, starting at $c < 0.5/S_l$ for the symmetric sperm, increasing rapidly at $b \approx 4\%$ to curvatures around $2/S_l$. The trajectory looks helical if the average curvature is larger then $1/S_l$, while curvatures smaller then $1/S_l$ are generally found if the trajectory is rather straight. Stronger curvature is found for sperm with a significant bent in the tail. This bent is generated dynamically for $b > 4\%$. In this case, the thrust of the tail and the drag force of the head induce the twisting and bending of the axoneme out of the beating plane. With careful observation this twist can also be seen in Fig. 4.

This rapid change in the tail curvature also effects other swimming parameters, like the rotation frequency. The rotation frequency at first increases with the bending parameter, but as the sperm is deformed, rotation slows down. The elastic deformation of the tail increases its asymmetry, so that the head bends even further out of the beating plane, thereby slowing down the rotational motion.

6 Outlook

The natural extension of this work is to look at hydrodynamic interactions of active objects. The first such question is what happens in the presence of walls. It is known for quite some time[17] that sperm cells accumulate at the walls of an observation chamber. Preliminary

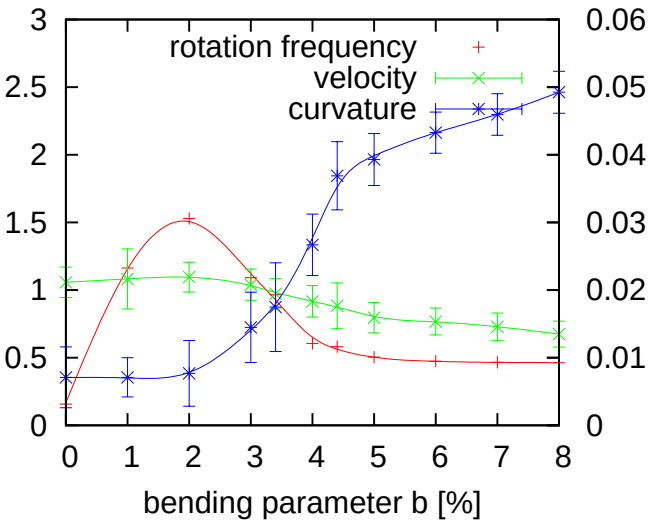

Figure 5. Parameters of helical sperm trajectories as a function of bending parameter b. All quantities are measured in units of sperm length S_l and beat period τ_b. Curvature is given in units of $1/S_l$ (left scale), rotation frequency in units of $2\pi/\tau_b$ (right scale), and swimming velocity in units of S_l/τ_b (right scale)

simulation results show that hydrodynamic interactions are sufficent to cause an effective attraction of sperm cells to walls.

The true strength of this simulation scheme is the possibility to simulate several interacting active objects. Large arrays of biological cilia display metachronal waves. We have simulated large arrays of cilia and have shown that hydrodynamics is sufficient to cause a self-organized metachronal coupling. Furthermore we could show that this metachronal wave enhances fluid transport and efficiency by almost an order of magnitude.

Acknowledgments

We thank NIC for providing computational resources on JUMP. Helpful discussions with U.B. Kaupp are gratefully acknowledged.

References

1. E. M. Purcell. Life at low Reynolds-number. *Am. J. Phys.*, **45**:3–11, 1977.
2. `http://physics.nyu.edu/pine/research/hydroreverse.html`.
3. T. Strunker, I. Weyand, W. Bonigk, Q. Van, A. Loogen, J. E. Brown, N. Kashikar, V. Hagen, E. Krause, and U. B. Kaupp. A K+-selective cGMP-gated ion channel controls chemosensation of sperm. *Nature Cell Biol.*, **8**:1149, 2006.
4. A. Malevanets and R. Kapral. Mesoscopic model for solvent dynamics. *J. Chem. Phys.*, **110**:8605–8613, 1999.

5. A. Lamura, G. Gompper, T. Ihle, and D. M. Kroll. Multi-particle collision dynamics: Flow around a circular and a square cylinder. *Europhys. Lett.*, **56**:319–325, 2001.
6. T. Ihle and D. M. Kroll. Stochastic rotation dynamics: A Galilean-invariant mesoscopic model for fluid flow. *Phys. Rev. E*, **63**:020201, 2001.
7. M. Ripoll, K. Mussawisade, R. G. Winkler, and G. Gompper. Low-Reynolds-number hydrodynamics of complex fluids by multi-particle collision dynamics. *Europhys. Lett.*, **68**:106–112, 2004.
8. M. Ripoll, K. Mussawisade, R. G. Winkler, and G. Gompper. Dynamic regimes of fluids simulated by multiparticle-collision dynamics. *Phys. Rev. E*, **72**:016701, 2005.
9. T. Ihle and D. M. Kroll. Stochastic rotation dynamics. I. Formalism, Galilean invariance, and Green-Kubo relations.
10. M. Ripoll, R. G. Winkler, and G. Gompper. Star polymers in shear flow. *Phys. Rev. Lett.*, **96**:188302, 2006.
11. H. Noguchi and G. Gompper. Fluid vesicles with viscous membranes in shear flow. *Phys. Rev. Lett.*, **93**:258102, 2004.
12. H. Noguchi and G. Gompper. Shape transitions of fluid vesicles and red blood cells in capillary flows. *P. Natl. Acad. Sci. USA.*, **102**:14159, 2005.
13. A. Malevanets and J. M. Yeomans. Dynamics of short polymer chains in solution. *Europhys. Lett.*, **52**:231–237, 2000.
14. M. M. Tirado, C. L. Martinez, and J. G. Delatorre. Comparison of theories for the translational and rotational diffusion-coefficients of rod-like macromolecules - application to short DNA fragments. *J. Chem. Phys.*, **81**:2047–2052, 1984.
15. J. Gray and G. J. Hancock. The propulsion of sea-urchin spermatozoa. *J. Exp. Biol.*, **32**:802–814, 1955.
    Phys. Rev. E, **67**:066705, 2003.
16. W. Humphrey, A. Dalke, and K. Schulten. VMD – Visual Molecular Dynamics. *Journal of Molecular Graphics*, **14**:33–38, 1996.
17. L. Rothschild. Non-random distribution of bull spermatozoa in a drop of sperm suspension. *Nature*, **198**:1221, 1963.